


Magnetoelectrically Controlled Valley Filter and Valley Valve in Bilayer Graphene

Changsoo Park*

Department of Physics, Dankook University, Cheonan 31116, Republic of Korea

 (Received 17 October 2018; revised manuscript received 20 February 2019; published 11 April 2019)

We study the effects of inversion asymmetry and tunable band gap on the transmission of particles in bilayer graphene junctions to propose a model for a valley-filter and valley-valve device. The device is made up of a series of two n - p - n (or p - n - p) junctions produced by electric gate potentials: one of them, being applied by an out-of-layer magnetic field, functions as a valley filter and the other as a valley valve. The valley filtering is based on the valley-dependent Zeeman interaction between the applied magnetic field and the orbital magnetic moment that can exist in a system with broken inversion symmetry. The valley valve is performed by varying the size of band gap via the gate potential that controls the flow of valley-polarized particles. We demonstrate that the device can achieve nearly perfect valley polarization and very high efficiency of valley-valve effect. By fixing magnetic field, the device can be operated by electric gate potentials only, and the tunable band gap makes a continuous control of valley-separate switching on and off possible.

DOI: [10.1103/PhysRevApplied.11.044033](https://doi.org/10.1103/PhysRevApplied.11.044033)

I. INTRODUCTION

Devising a valley-dependent electronic device by managing valley degree of freedom (VDF) in graphene and other two-dimensional materials with hexagonal lattice structure, called valleytronics, has attracted much interest in recent years [1–7]. The primary requirement for realizing such a device is to generate valley-polarized particles by lifting the intrinsic valley degeneracy of K and K' valleys, which are symmetric under time reversal. Various theoretical schemes of valley filtering [8–38] based on breaking the time-reversal symmetry and/or inversion symmetry and some experimental results [39–42] have been reported. For practical use of a valleytronic device such as valley logic gates that employ valley-dependent information, however, it is also desirable to construct a combined unit of valley filter and valley valve [7,8]. In this regard, one of the main concerns is to design a device that can manipulate the VDF in a simplified and viable way to produce valley-dependant information. While there are a large number of proposals for the mechanism of valley filtering, practical models for such a combined device implementing both functions and satisfying the demands are currently limited [8,9,34].

In this paper, we propose a model with bilayer graphene (BLG) that can perform both valley filter and valley valve as a single system. As illustrated in Fig. 1, the valley-filter and -valve device consists of a series of two electric gates

V_{G1} and V_{G2} (with corresponding voltages V_{g1} and V_{g2}), applying an out-of-layer magnetic field $\mathbf{B} = B\hat{\mathbf{e}}_z$ to the first gate. Potential barriers (n - p - n) or wells (p - n - p) can be constructed by using the electric gates [43]. The first (with magnetic field) and second gates, respectively, function as a valley filter and a valley valve.

The operation of the device exploits two important outcomes of applying gate voltages: breaking the inversion symmetry and opening a tunable band gap [43–48]. In a system with broken inversion symmetry, an intrinsic orbital magnetic moment due to the self-rotation of the wavepacket of a band electron exists [2]. In BLG this magnetic moment depends on the VDF, with opposite directions for K and K' valleys [see Eq. (5) below]. In the presence of an external magnetic field the orbital magnetic moment undergoes Zeeman-like interaction, which breaks the time-reversal symmetry and causes energy split to band energy because of the opposite polarity of the two valleys [3,49]. The valley filter in the first gate V_{G1} is based on this valley-dependent Zeeman (VZ) splitting: when the incident energy coincides with the edge of the band in a barrier or well the energy of one valley may lie inside a band gap, while that of the other valley remains within a band (see region II of the top and bottom panels in Fig. 1). The transmission of particles in the band gap is greatly suppressed due to the absence of states, but the particles inside the band pass through the barrier or well with high probability due to the chiral tunneling, exhibiting valley filtering.

The transmitted valley-polarized particles then enter the second gate V_{G2} where band gap is tuned by the gate

*olnal@dankook.ac.kr.

voltage V_{g2} . Here, the valley valve is performed by controlling the transport of valley-polarized particles with the size of band gap (see region IV in Fig. 1): if the gap is large enough so that the energy of the polarized particles lies within the band gap the transmission is again greatly suppressed, but for small gap the energy can be located inside the band where the particles are readily conveyed via the chiral tunneling. As a result, the transmission of valley-polarized particles in a large gap becomes much smaller than in a small gap, giving rise to valley-valve effect. In the following, we demonstrate that nearly perfect valley polarization from the first gate and very high efficiency of valley-valve effect from the second gate can be achieved.

II. VALLEY FILTERING AND VALLEY-VALVE EFFECT

A. Model and formulation

As illustrated in Fig. 1, we consider a BLG with armchair edges (along the x direction) to avoid possible edge states within band gap (see the discussion in Sec. II C) [50,51]. With this arrangement our model can be represented by the Hamiltonian

$$\hat{\mathcal{H}} = \hat{\mathcal{H}}_0 + sU_1(x) + sU_2(x) + U_{Z\tau}(x). \quad (1)$$

Here, $\hat{\mathcal{H}}_0$ is the effective two-band Hamiltonian of BLG [44], which, in the presence of magnetic field, is expressed as

$$\hat{\mathcal{H}}_0 = \begin{bmatrix} \Delta/2 & (v_F^2/\gamma_1) \Pi_-^2 \\ (v_F^2/\gamma_1) \Pi_+^2 & -\Delta/2 \end{bmatrix}, \quad (2)$$

where $\gamma_1 \approx 0.4$ eV (interlayer nearest-neighbor hopping), $v_F \approx 10^6$ m/s (Fermi velocity), $\Pi_{\pm} = \tau p_x \pm i[p_y + eA(x)]$ ($p_{x,y} = -i\hbar\partial_{x,y}$) with τ being the valley index ($\tau = +1$ for K valley and $\tau = -1$ for K' valley). We choose Landau gauge

$$\mathbf{A}(x) = Bx\Theta(d^2/4 - x^2)\hat{\mathbf{e}}_y \pm (Bd/2)\Theta(\pm x - d/2)\hat{\mathbf{e}}_y, \quad (3)$$

where $\Theta(x)$ is the Heaviside step function (taking $x = 0$ at the center of region II) and the double signs are in the same order, so that the magnetic field becomes $\mathbf{B}(x) = \nabla \times \mathbf{A}(x) = B\Theta(d^2/4 - x^2)\hat{\mathbf{e}}_z$. The two electric gates V_{G1} and V_{G2} can produce a series of two potential barriers or wells $sU_1(x)$ and $sU_2(x)$, where $U_1(x) = U_0\Theta(d^2/4 - x^2)$ and $U_2(x) = U\Theta[d^2/4 - (x - a - d)^2]$ with $U_0 = eV_{g1}$ and $U = eV_{g2}$ ($e > 0$) [52] and the index s depicts the type of potential: $s = +1$ for barrier and $s = -1$ for well. They also determine the band-gap parameter Δ [43]: we label the gap size at each gate by Δ_1 and Δ_2 , respectively. The last term $U_{Z\tau}(x)$ is the VZ energy due to the coupling of

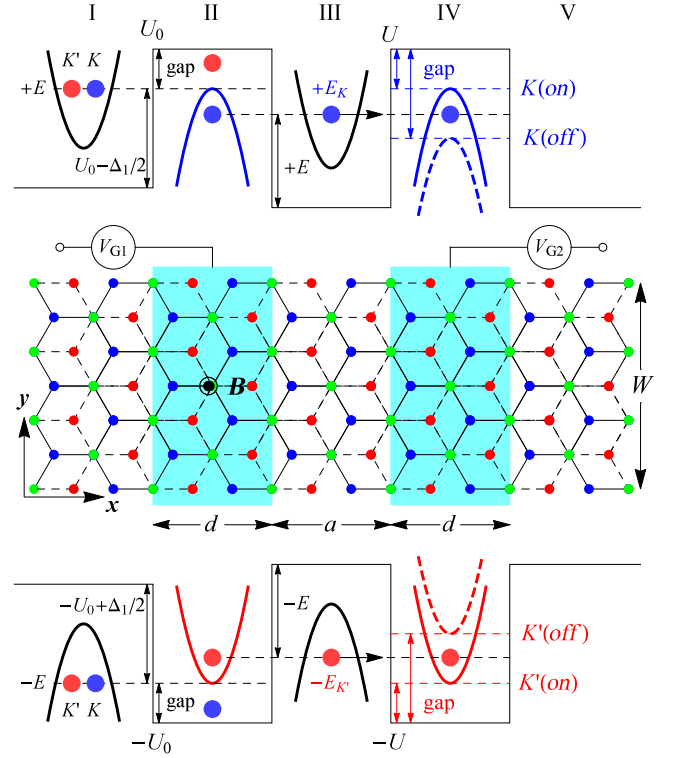


FIG. 1. Operation of valley filter and valley valve in bilayer graphene with armchair edge. Middle: schematic of a valley-filter and -valve device composed of two electric gates V_{G1} (with out-of-layer magnetic field $\mathbf{B} = B\hat{\mathbf{e}}_z$) and V_{G2} . Top and bottom panels, respectively, show potential profiles of barrier (n - p - n) and well (p - n - p). The first gate with magnetic field produces valley-polarized particles due to the valley Zeeman splitting when the incident energies $\pm E$ are tuned to the band edges: barrier and well filter off K' - and K -valley particles, respectively. The second gate controls the flow of valley-polarized particles by tuning the size of band gap: for small gap $+E_K$ and $-E_{K'}$ remain inside the band so that particles are well transmitted (*on* states), but for large gap they are placed outside the band and hence the transmission is suppressed (*off* states).

the orbital magnetic moment \mathbf{m}_τ to the external magnetic field \mathbf{B} , given as

$$U_{Z\tau}(x) = -\mathbf{m}_\tau \cdot \mathbf{B}(x) = \tau U_m \Theta(d^2/4 - x^2), \quad (4)$$

where $U_m = |\mathbf{m}_\tau \cdot \mathbf{B}|$ and \mathbf{m}_τ is defined as [1]

$$\begin{aligned} \mathbf{m}_\tau &= -i \frac{e}{2\hbar} \langle \nabla_k u_{s\tau}(\mathbf{k}) | \times \left[\hat{\mathcal{H}}_0(\mathbf{k}) - sE(\mathbf{k}) \right] | \nabla_k u_{s\tau}(\mathbf{k}) \rangle \\ &= -\tau \mu_B^* \frac{\Delta_1 \sqrt{E^2 - (\Delta_1/2)^2}}{E^2} \hat{\mathbf{e}}_z, \end{aligned} \quad (5)$$

with $|E| > \Delta_1/2$ and $\mu_B^* = e\hbar v_F^2/\gamma_1 \approx 1.7$ (meV/T) being the effective Bohr magneton. In the above equation $\hat{\mathcal{H}}_0(\mathbf{k}) = e^{-ik \cdot r} \hat{\mathcal{H}}_0 e^{ik \cdot r}$ with $B = 0$ in Eq. (2), satisfying the eigenvalue equation $\hat{\mathcal{H}}_0(\mathbf{k}) |u_{s\tau}(\mathbf{k})\rangle = sE(\mathbf{k}) |u_{s\tau}(\mathbf{k})\rangle$,

where $|u_{s\tau}(\mathbf{k})\rangle$ is the sublattice pseudospinor given by $|u_{s\tau}(\mathbf{k})\rangle = (1/\sqrt{2E}) (\sqrt{E + s\Delta_1/2}, -se^{2i\tau\phi}\sqrt{E - s\Delta_1/2})^T$ with T denoting transpose and $\phi = \arctan(k_y/k_x)$ being the incident angle and $E(\mathbf{k}) = \sqrt{(\hbar^2 v_F^2 k^2 / \gamma_1)^2 + (\Delta_1/2)^2}$ with $k^2 = k_x^2 + k_y^2$. Note that the magnetic moment has maximum value $|\mathbf{m}_\tau| = \mu_B^*$ when $E = \Delta_1/\sqrt{2}$. The spin Zeeman energy is neglected because it is much smaller than the VZ energy [2]: the effective Bohr magneton with given values of γ_1 and v_F of BLG is $\mu_B^* \simeq 31\mu_B$, where $\mu_B = e\hbar/2m_e$ is the Bohr magneton of the bare electron.

We solve the wave equation $\hat{\mathcal{H}}|\psi_{s\tau}(\mathbf{r})\rangle = sE|\psi_{s\tau}(\mathbf{r})\rangle$ by using the method of transfer matrix, where $|\psi_{s\tau}(\mathbf{r})\rangle = |u_{s\tau}\rangle\varphi(\mathbf{r})$ with $\varphi(\mathbf{r}) \propto e^{i\mathbf{k}\cdot\mathbf{r}}$ [$\mathbf{k} = (k_x, k_y)$ and $\mathbf{r} = (x, y)$], to calculate valley-dependent transmission probability in each gate [38]. We then obtain valley-dependent conductance through each gate by using

$$G_{i\tau} = G_0 \int_{-\phi_c}^{\phi_c} |T_{i\tau}(\phi)|^2 \frac{k_{x+}(\phi)}{k_{x-}(\phi)} \cos \phi d\phi \quad (i = 1, 2), \quad (6)$$

where $T_{i\tau}$ are the transmission coefficients, $G_0 = g_s e^2 k W / 2\hbar\phi_c$ with $g_s = 2$ (spin factor), ϕ is the incident angle, $\phi_c = \arcsin(1 - eBd/2\hbar k)$ is the critical angle of incident wave due to the cyclotron motion inside the barrier and well region [53,54], and $k_{x\pm}(\phi) = k\sqrt{1 - (\sin\phi \pm eBd/2\hbar k)^2}$ with $k = \sqrt{\gamma_1(E^2 - \Delta_1^2/4)^{1/4}/\hbar v_F}$ are the x components of wave vectors for incident (k_{x-}) and transmitted (k_{x+}) waves in the first gate: for the second gate we use k_{x+} both in regions III and V.

B. Valley filter

The valley filtering by the first gate V_{G1} can be explained as follows. The wave equation for the barrier or well in V_{G1} is $(\hat{\mathcal{H}}_0 + sU_1)|\psi_{1s\tau}(\mathbf{r})\rangle = sE_\tau|\psi_{1s\tau}(\mathbf{r})\rangle$, where $U_1 = U_0$ and $E_\tau = E - s\tau U_m$ with $s\tau = (\pm 1) \times (\pm 1)$ is an effective energy incorporating the VZ effect. When the incident energy E coincides with the band edge (i.e., $E = U_0 - \Delta_1/2$), which we refer to as band-edge tunneling (BET), the effective energy becomes $E_\tau = U_0 - \Delta_1/2 - s\tau U_m$. Thus, when $s\tau > 0$ the effective energy E_τ is less than $U_0 - \Delta_1/2$ so that it lies within the band. On the other hand, when $s\tau < 0$ the effective energy becomes larger than $U_0 - \Delta_1/2$ and hence it enters the band gap. This implies that in the barrier (well) region $K(K')$ -valley particles remain inside the band and $K'(K)$ -valley particles are pushed outside the band (see region II in Fig. 1): hereafter we use K or K' particles, omitting valley. As a consequence, in the barrier (well), the $K(K')$ particles are well transmitted while the transmission of $K'(K)$ particles is suppressed.

More explicitly, we can rewrite the wave equation as $\hat{\mathcal{H}}_0|\psi_{1s\tau}(\mathbf{r})\rangle = s(E_\tau - U_0)|\psi_{1s\tau}(\mathbf{r})\rangle \equiv sE_1(\mathbf{k})|\psi_{1s\tau}(\mathbf{r})\rangle$,

where $E_1(\mathbf{k}) = \sqrt{(\hbar^2 k^2 / 2m^*)^2 + (\Delta_1/2)^2}$ is an effective eigenspectrum with $m^* = \gamma_1/2v_F^2$ and $k = \sqrt{k_x^2 + (k_y + eBx/\hbar)^2}$ being the wave vector inside the first barrier or well region. From this, using $E_\tau = U_0 - \Delta_1/2 - s\tau U_m$ for BET with VZ effect, we can obtain the x component of the wave vector for transmitting wave $\varphi(\mathbf{r}) \propto e^{ik_x x}$ as

$$k_x^2 = \pm \frac{\gamma_1}{\hbar^2 v_F^2} \sqrt{U_m(U_m + s\tau\Delta_1)} - \left(k_y + \frac{eB}{\hbar}x\right)^2, \quad (7)$$

where, from the conservation of transverse momentum, $k_y = k_{\text{in}} \sin\phi$ with $k_{\text{in}} = [\gamma_1^2 U_0(U_0 - \Delta_1)]^{1/4}/\hbar v_F$ for BET. Assuming $\Delta_1/2 > U_m$, the wave vector k_x becomes complex when $s\tau < 0$ (outside the band), yielding oscillating waves, but with evanescent amplitudes, which results in suppressed transmission. When $s\tau > 0$ (inside the band), however, k_x^2 is real and hence pure oscillating or evanescent waves exist, which, in association with the pseudospinor $|u_{s\tau}\rangle$, leads to the chiral tunneling [55,56] with high transmission probability. Consequently, the barrier (well) transmits $K(K')$ particles, while filtering off $K'(K)$ particles.

To see the valley-filter effect we calculate the conductances G_{1K} and $G_{1K'}$ through the first gate V_{G1} using Eq. (6). The capability of valley filtering can be characterized by the degree of valley polarization, defined as

$$\mathcal{P} = \frac{|G_{1K} - G_{1K'}|}{G_{1K} + G_{1K'}}. \quad (8)$$

In this calculation, since the magnetic moment \mathbf{m}_τ in Eq. (5) has maximum value when $E = \Delta_1/\sqrt{2}$, we choose the incident energy of BET to be $E = U_0 - \Delta_1/2 = \Delta_1/\sqrt{2}$ to maximize the effect of VZ interaction. This gives $U_m = \mu_B^* B$, $\Delta_1 = 2(\sqrt{2} - 1)U_0$, and $E = (2 - \sqrt{2})U_0$ from which the incident wave vector becomes $k = (\sqrt{2} - 1)^{1/2} \sqrt{\gamma_1 U_0}/\hbar v_F$. The control parameters are thus reduced to U_0 and B if the width of potential d and sample width W are fixed. In Fig. 2 we present the degree of polarization \mathcal{P} as a function of U_0 for two different magnetic fields. As we can see, the ability of valley filter is very high, reaching almost 100% in the range of $U_0 \gtrsim 100$ meV: note that both barrier and well have $\mathcal{P} \simeq 1$ in this range. The results clearly show that nearly perfect valley filtering of K or K' particles can be achieved from the first gate.

The two parameters U_0 and B are determined by the gate voltage V_{g1} and the external magnetic field \mathbf{B} , respectively. If the direction of magnetic field is reversed the roles of barrier and well are also reversed because the sign of $U_{Z\tau}$ is changed: note that each potential type can generate both K and K' particles by reversing the magnetic field (see Table I). Thus, we have two choices to generate valley-polarized particles, either by changing the type of potential

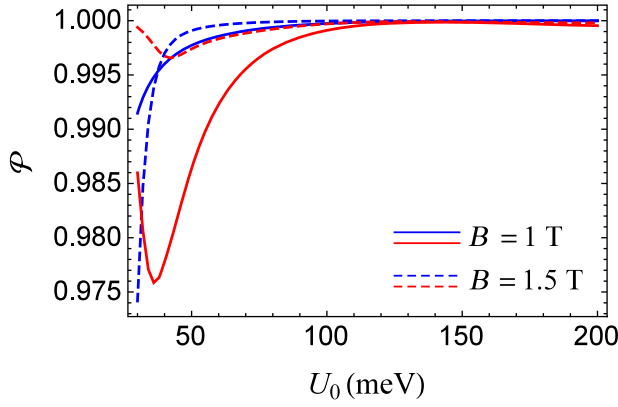


FIG. 2. Degree of polarization $\mathcal{P} = |G_{1K} - G_{1K'}| / (G_{1K} + G_{1K'})$ as a function of the height and depth of the potential barrier or well U_0 in the first gate V_{G1} when $d = 50$ nm. Blue and red curves represent barrier and well, respectively.

via the gate voltage V_{g1} while fixing the magnetic field or vice versa. For device application it is more favorable to fix magnetic field (either $\mathbf{B} = +B\hat{e}_z$ or $-B\hat{e}_z$) so that only the electric control of U_0 is necessary. We shall return to this point later in conjunction with the valley-valve effect.

C. Valley valve

We now consider the valley-valve effect in the second gate V_{G2} . The transmitted K or K' particles from the first gate have effective energies sE_τ ($s = \pm$ and $\tau = K, K'$), which now become incident energies for the second gate where the size of band gap Δ_2 can be tuned by the gate voltage V_{g2} . Here, as in the first gate, depending on whether sE_τ is located inside or outside the band, contrasting transmission probabilities of valley-polarized particles appear.

To illustrate how the flow of valley-polarized particles through V_{G2} is controlled by the size of gap we first examine the wave equation for the second potential barrier or well, $(\hat{\mathcal{H}}_0 + sU_2)|\psi_{s\tau}\rangle = sE_\tau|\psi_{s\tau}\rangle$, where $\hat{\mathcal{H}}_0$ is given in Eq. (1) with $A(x) = Bd/2$ and $U_2 = U$. Rearranging terms, the effective wave equation can be written as $\hat{\mathcal{H}}_0|\psi_{2s\tau}\rangle = s(E_\tau - U_2)|\psi_{2s\tau}\rangle \equiv E_2(\mathbf{k})|\psi_{2s\tau}\rangle$, where $E_2(\mathbf{k}) = \sqrt{(\hbar^2 k^2 / 2m^*)^2 + (\Delta_2/2)^2}$ with $k = \sqrt{k_x^2 + (k_y + eBd/2\hbar)^2}$. To proceed we adjust the effective energy sE_τ to sE by lowering (raising) the reference of barrier (well) (see region III in Fig. 1). In addition,

TABLE I. Summary of valley polarization from the gate V_{G1} . The direction of magnetic field is determined by $\mathbf{B} = \pm B\hat{e}_z$.

Barrier ($n-p-n$)		Well ($p-n-p$)	
$+B$	$-B$	$+B$	$-B$
K	K'	K'	K

we also choose $U = U_0 + U_m$ ($U_m = \mu_B^* B$) for the height and depth of the second potential barrier or well [57]. For BET with maximum VZ effect this gives $E_\tau = E = (2 - \sqrt{2})U_0$. The transition from inside to outside of the band occurs when $\Delta_2/2 = U - E \equiv \Delta_t/2$, from which the transition gap is $\Delta_t/2 = (\sqrt{2} - 1)U_0 + U_m$. With these choices the x component of the wave vector in the gate V_{G2} is obtained as

$$k_x^2 = \pm \frac{\gamma_1}{2\hbar^2 v_F^2} \sqrt{\Delta_t^2 - \Delta_2^2} - \left(k_y + \frac{eBd}{2\hbar} \right)^2. \quad (9)$$

Thus, when $\Delta_2 < \Delta_t$ (inside the band) the wave vector k_x becomes real to have high transmission probability due to the chiral tunneling. When $\Delta_2 > \Delta_t$ (outside the band), however, the wave vector becomes complex to produce oscillating waves with evanescent amplitudes and hence the transmission is suppressed (see region IV in Fig. 1).

Based on above analysis we compute the transmission probability as a function of the size of band gap Δ_2 . In Fig. 3, we show the density plots of transmission probabilities $|T_{2\tau}(\phi, \Delta_2/2)|^2$ for potential barrier (K particles) and well (K' particles). A significant change of probability at Δ_t (indicated by red arrows) is clearly seen. To elucidate the contrast of transports between inside and outside the band we also calculate the conductance $G_{2\tau}$ in the second gate by using Eq. (6): note $k_{x+}/k_{x-} = 1$ in this case. The results are presented in Figs. 4(a), 4(b), and 5, from which it is observed that the conductance drops drastically near the transition gap Δ_t (indicated by arrows). This manifests the valley-valve effect of the second gate V_{G2} . The efficiency of valley valve may be further illustrated by the relative change of conductances inside and outside the band, defining it as follows [58]:

$$\eta = \frac{\langle G_{2in} \rangle - G_{2out}}{G_{2out}}, \quad (10)$$

where $\langle G_{2in} \rangle$ is an average conductance over the range of Δ_2 for $\Delta_2 < \Delta_t$ (inside the band) and G_{2out} are the conductances when $\Delta_2 > \Delta_t$ (outside the band): note that the range of Δ_2 is $|\Delta_2 - \Delta_t| < \Delta_t$. As an example, Fig. 4(c) shows the ratio η when $U_0 = 100$ meV and $B = 1$ T. As expected from Figs. 4(a) and 4(b) the relative ratio is very large, ranging $10^2 \lesssim \eta \lesssim 10^5$ (more than 10⁴%), which confirms very high efficiency of the valley-valve effect from the second gate. Incidentally, we also observe from Fig. 5 that the high efficiency of valley valve is insensitive to the interpotential distance a .

The suppression of transport inside the band gap can be examined qualitatively by using the WKB approximation. The WKB transmission probability in the gate V_{G2} can be obtained from the transmission coefficient $T_{\text{WKB}} \propto e^{\delta_{\text{WKB}}}$, where $\delta_{\text{WKB}} = i \int_{x_i}^{x_f} k_x dx$ is the WKB phase with $x_i = a + d/2$ and $x_f = a + 3d/2$ and k_x being given in Eq.

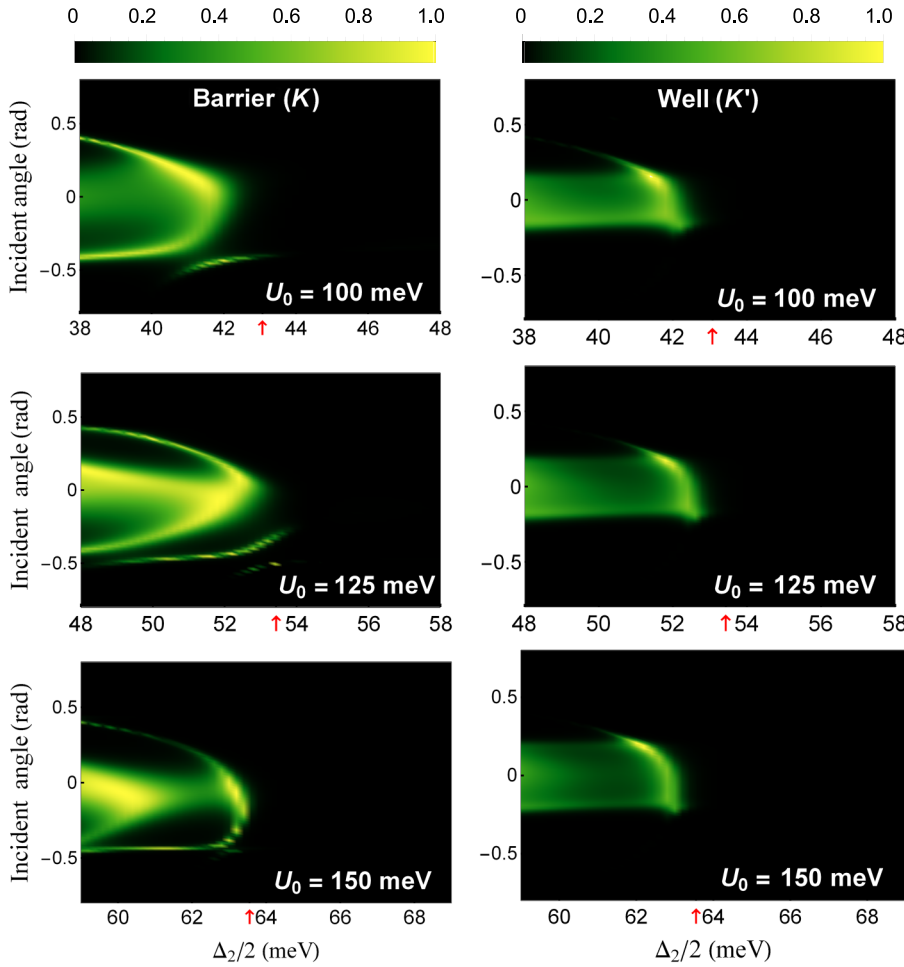


FIG. 3. Transmission probability $|T_{2\tau}(\phi, \Delta_2/2)|^2$ of valley-polarized particles in the second gate V_{G2} : barrier for K particles and well for K' particles. Red arrows indicate the gap Δ_t at which transition from the inside to the outside of the band occurs, given by $\Delta_t/2 = (\sqrt{2} - 1)U_0 + U_m$ ($U_m = \mu_B^*B$). Parameters are $d = 50$ nm, $a = 20$ nm, and $B = 1$ T.

(9). Collecting the leading-order terms in Δ_2 the transmission probability for forward transport can be approximated as [60] $P_{\text{WKB}} \propto |T_{\text{WKB}}|^2 \sim \exp(-\alpha d \sqrt{\Delta_2})$, where $\alpha = (4\gamma_1/\hbar^2 v_F^2)^{1/2}$ and $\Delta_2 > \Delta_t$. From Eq. (6) the leading-order behavior of conductance is thus $G_{2\tau} \propto P_{\text{WKB}}$. This shows that the width d is a dominant factor for the suppression, suggesting greater suppression with larger width of potential. When the width d is fixed the conductance decays exponentially with the size of band gap Δ_2 , which is consistent with the results in Fig. 4 for large Δ_2 .

We discuss here some points relevant to experimental realization of the present model. First, the arrangement of the sample used here is a BLG with armchair edges. It has been reported that for a BLG nanoribbon with zigzag edges there exist dispersive edge states around K and K' valleys within band gap [50,51], which may serve as transmission channels for particles within band gap. Since our model requires a band gap that suppresses transmission it is thus preferable to use the arrangement with armchair edges, which has no edge states within band gap.

As a second point, we use idealized rectangular potentials with sharp boundaries. For smooth boundaries, which is closer to a real experiment, the profile of transmission

probabilities inside the band changes (see, for example, Ref. [61]). This may alter the transmission probabilities, variation of conductances, and the position of transition gap Δ_t in Figs. 3 and 4, but the contrasting behavior of transmission probabilities between inside and outside the band is still maintained, which can preserve the large relative change of conductances in Eq. (10). Thus, the high efficiency of valley-valve effect is expected even in smooth variation of potentials.

Finally, we estimate the possible temperature range in which the present model is valid. For this we first note that the applied magnetic field bend the particle's path inside the potential region II because of the cyclotron motion, which restricts the allowed range of magnetic field. Following Refs. [53] and [54], there exist a critical field for nonvanishing transmission, which can be determined by the condition $|\sin \phi| \lesssim eBd/2\hbar k < 1$. From this, for BET and maximum VZ effect, the critical field can be obtained as $B_c \simeq 1.287\sqrt{\gamma_1 U_0}/edv_F$. The corresponding VZ energy is then $U_{mc} = \mu_B^* B_c \simeq (1.287\hbar v_F/d)\sqrt{U_0/\gamma_1}$. In order for thermal energy not to wash out the valley filtering this should satisfy $k_B T < U_{mc} = k_B T_c$, from which we can define a valid temperature range of the present model as

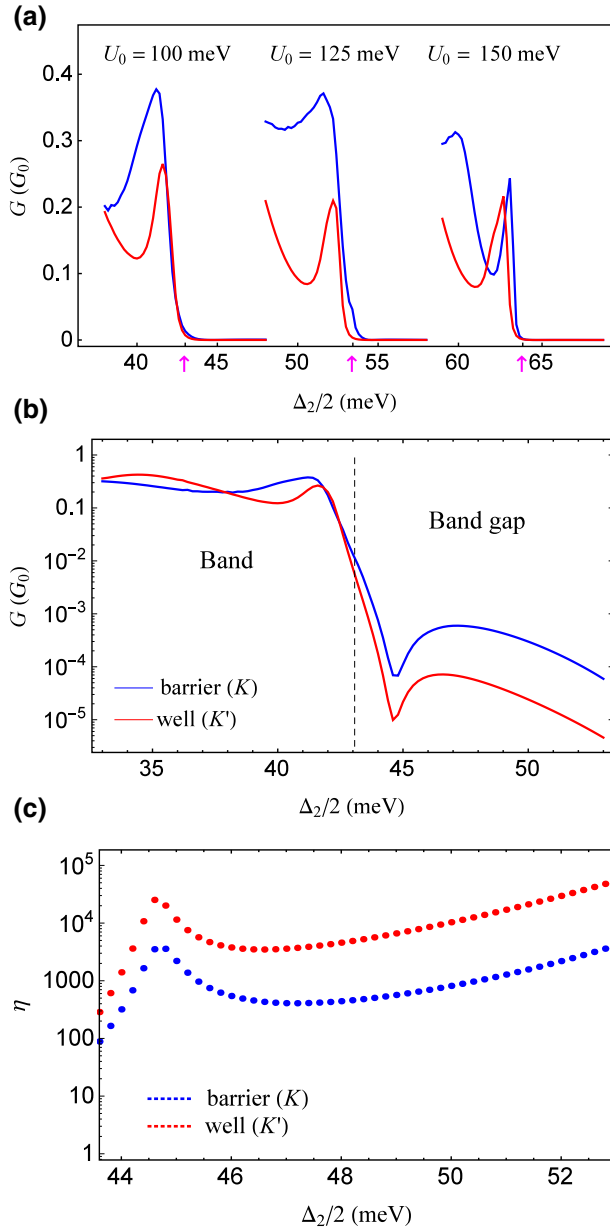


FIG. 4. (a) Variation of conductance in the second gate as a function of band gap Δ_2 for barrier (K , blue) and well (K' , red) with height and depth $U = U_0 + U_m$ ($U_m = \mu_B^* B$). Arrows indicate the transition gap Δ_t as in Fig. 3. Note the abrupt change near Δ_t . Log plots of (b) conductance and (c) relative change of conductance $\eta = (G_{2in} - G_{2out})/G_{2out}$ when $U_0 = 100$ meV. The dashed line in (b) indicates Δ_t . Parameters and units are as follows: $a = 20$ nm, $d = 50$ nm, $B = 1$ T, and $G_0 = e^2 k W / h \phi_c$ with $\phi_c = \arcsin(1 - e B d / 2 \hbar k)$ and $k = (\sqrt{2} - 1)^{1/2} \sqrt{\gamma_1 U_0} / \hbar v_F$ [59].

$T < T_c$ with $T_c = (1.287 \hbar v_F / k_B d) \sqrt{U_0 / \gamma_1}$. Note that both B_c and T_c depend on the parameters of potential barrier or well U_0 and d . Using $\Delta_1/2 = (\sqrt{2} - 1)U_0$ the maximum allowed value of U_0 is, from $\Delta_{\max} \simeq 250$ meV [46], $U_0^{\max} \simeq 300$ meV. As a numerical example, for $d = 50$ nm

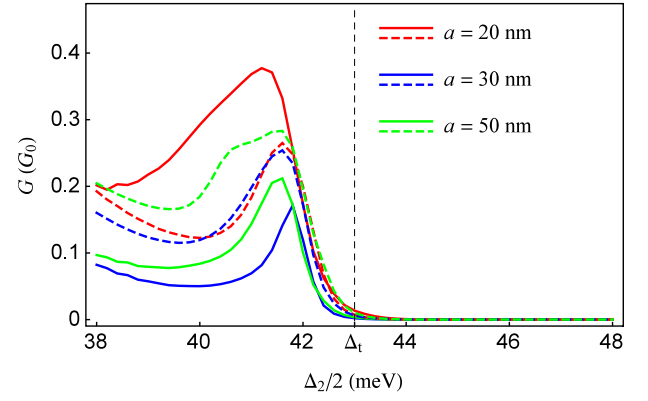


FIG. 5. Variation of conductance in the second gate as a function of band gap Δ_2 for barrier (K , solid curves) and well (K' , dashed curves) with different inter-potential distances of a . Parameters and units are as follows: $U_0 = 100$ meV, $d = 50$ nm, $B = 1$ T, and $G_0 = e^2 k W / h \phi_c$ with $\phi_c = \arcsin(1 - e B d / 2 \hbar k)$ and $k = (\sqrt{2} - 1)^{1/2} \sqrt{\gamma_1 U_0} / \hbar v_F$ [59].

and $50 \text{ meV} \leq U_0 \leq 300 \text{ meV}$, we can estimate the range of critical fields and temperatures as $4 \text{ T} \lesssim B_c \lesssim 10 \text{ T}$ and $70 \text{ K} \lesssim T_c \lesssim 170 \text{ K}$. Noticing $T_c \propto 1/d$, the lower and upper bounds of T_c can be increased by decreasing the potential width d .

D. Electrical control and valley-separate switch

As mentioned earlier, for device application, it is preferable to have all-electrical control of valley-filter and valley-valve effects. Although our model employs both electric and magnetic fields it should be noted that the magnetic field \mathbf{B} can be readily fixed by contacting a ferromagnet with easy axis perpendicular to the layer in the region of the first gate [62–64]. In this case, as shown in Fig. 1, the valley polarization is determined by the height (depth) of the barrier (well) U_0 , which is controlled by the electric gate voltage V_{g1} . As discussed above, the band gap Δ_2 in the second gate is tuned by the gate potential V_{g2} . Thus, the two functions of valley filter and valve can be controlled by the two electric gate potentials only, making all-electrical control possible. Moreover, by choosing U_0 with a high degree of polarization from Fig. 1, we can also fix U_0 , so that the size of band gap Δ_2 in the second gate becomes the only controlling parameter.

We remark here that each of the two gates plays a distinct role, one for valley filter and the other for valley valve. This is different from other proposals [8,34] in which a series of two valley filters performs a valve by arranging them in opposite valley polarizations. The valley-valve effect in our model is carried out solely in the second gate by tuning the size of band gap Δ_2 . In addition, the gap can be continuously tuned across the transition gap Δ_t in the range of $|\Delta_2 - \Delta_t| < \Delta_t$, which

makes a continuous control of valley-separate switching on and off possible (see regions VI and V in Fig. 1). Since each of the barrier and well can produce both K and K' particles by using opposite directions of \mathbf{B} (see Table I) the valley-separate switching effect can be implemented in each potential type.

Finally, we comment on the possible application of the present model to classical logic gates, in particular the NAND gate, which is a universal gate; but it is irreversible because the input to output is a two-to-one type. Recently, the authors in Ref. [34] showed that the two valley-polarized states together with null polarization can be used as information storage to produce a *reversible* NAND gate: by labeling each of the three output-*on* states and one output-*off* state with extra index such as $(1, K)$, $(1, K')$, $(1, \text{null})$, and $(0, 0)$ the NAND gate can be expressed as a 4×4 matrix because it becomes two-to-two type between input and output. In our model, the null-polarized particles can be generated from the first gate when $\mathbf{B} = 0$ so that no polarization occurs because of zero VZ splitting. In this case the first gate serves directly as a valve by tuning the band gap Δ_1 just like in the second gate: for small gap such that $|E| < |U_0 - \Delta_1/2|$ (inside the band) null-polarized particles are well transmitted and for large gap such that $|E| > |U_0 - \Delta_1/2|$ (outside the band) the transmission is suppressed. Thus, with zero magnetic field, one electrical gate is enough to generate the null polarization and perform the valve. This suggests that it is also possible to make the *reversible* NAND gate with the present model, and with fixed magnetic field ($\pm\mathbf{B}$ or $\mathbf{0}$) it can be implemented by electrical gates.

III. CONCLUSION

In conclusion, we demonstrate that a valley-filter and valley-valve device with bilayer graphene can be constructed by exploiting the valley-Zeeman splitting and tunable band gap. The valley-Zeeman splitting comes from the coupling of the valley-dependent orbital magnetic moment to the external magnetic field and leads to the valley-filter effect. The tunable band gap, produced by the electric gate voltage, is responsible for the valley-valve effect. The device exhibits very high efficiency of valley-valve effect as well as nearly perfect valley polarization. With fixed magnetic field the two functions are controlled solely by electric gate potentials. The continuous tunability of band gap and high efficiency make it possible for the valley valve to be used as a valley-dependent switch.

ACKNOWLEDGMENTS

The present work is supported by the research fund of Dankook University (Grant No. R-2018-00338).

-
- [1] Di Xiao, Wang Yao, and Qian Niu, Valley-Contrasting Physics in Graphene: Magnetic Moment and Topological Transport, *Phys. Rev. Lett.* **99**, 236809 (2007).
 - [2] Di Xiao, Ming-Che Chang, and Qian Niu, Berry phase effects on electronic properties, *Rev. Mod. Phys.* **82**, 1959 (2010).
 - [3] Xiaodong Xu, Wang Yao, Di Xiao, and Tony F. Heinz, Spin and pseudospins in layered transition metal dichalcogenides, *Nat. Phys.* **10**, 343 (2014).
 - [4] R. V. Gorbachev, J. C. W. Song, G. L. Yu, A. V. Kretinin, F. Withers, Y. Cao, A. Mishchenko, I. V. Grigorieva, K. S. Novoselov, L. S. Levitov, and A. K. Geim, Detecting topological currents in graphene superlattices, *Science* **346**, 448 (2014).
 - [5] Long Ju, Zhiwen Shi, Nityan Nair, Yinchuan Lv, Chenhao Jin, Jairo Velasco, Jr., Claudia Ojeda-Aristizabal, Hans A. Bechtel, Michael C. Martin, Alex Zettl, James Analytis, and Feng Wang, Topological valley transport at bilayer graphene domain walls, *Nature* **520**, 650 (2015).
 - [6] John R. Schaibley, Hongyi Yu, Genevieve Clark, Pasqual Rivera, Jason S. Ross, Kyle L. Seyler, Wang Yao, and Xiaodong Xu, Valleytronics in 2D materials, *Nat. Rev. Mater.* **1**, 16055 (2016).
 - [7] Seteven Vitale, Philip Kim, Nuh Gedik, Pablo Jarillo-Herrero, Di Xiao, and Dimitris Pavlidis, *Valleytronics materials, architectures, and devices workshop* (MIT Samberg Center, Cambridge, MA, 2017).
 - [8] A. Rycerz, J. Tworzydło, and C. W. J. Beenakker, Valley filter and valley valve in graphene, *Nat. Phys.* **3**, 172 (2007).
 - [9] Patrick Recher, Johan Nilsson, Guido Burkard, Björn Trauzettel, Bound states and magnetic field induced valley splitting in gate-tunable graphene quantum dots, *Phys. Rev. B* **79**, 085407 (2009).
 - [10] J. L. Garcia-Pomar, A. Cortijo, and M. Nieto-Vesperinas, Fully Valley-Polarized Electron Beams in Graphene, *Phys. Rev. Lett.* **100**, 236801 (2008).
 - [11] D. S. L. Abergel and T. Chakraborty, Generation of valley polarized current in bilayer graphene, *Appl. Phys. Lett.* **95**, 062107 (2009).
 - [12] J. M. Pereira, Jr., F. M. Peeters, R. N. Costa Filho, and G. A. Farias, Valley polarization due to trigonal warping on tunneling electrons in graphene, *J. Phys.: Condens. Matter* **21**, 045301 (2009).
 - [13] T. Fujita, M. B. A. Jalil, and S. G. Tan, Valley filter in strain engineered graphene, *Appl. Phys. Lett.* **97**, 043508 (2010).
 - [14] A. Chaves, L. Covaci, K. Y. Rakhimov, G. A. Farias, and F. M. Peeters, Wave-packet dynamics and valley filter in strained graphene, *Phys. Rev. B* **82**, 205430 (2010).
 - [15] Z. Wu, F. Zhai, F. M. Peeters, H. Q. Xu, and K. Chang, Valley-Dependent Brewster Angles and Goos-Hänchen Effect in Strained Graphene, *Phys. Rev. Lett.* **106**, 176802 (2011).
 - [16] D. Gunlycke and C. T. White, Graphene Valley Filter using a Line Defect, *Phys. Rev. Lett.* **106**, 136806 (2011).
 - [17] F. Zhai, Y. Ma, and K. Chang, Valley beam splitter based on strained graphene, *New J. Phys.* **13**, 083029 (2011).

- [18] L. E. Golub, S. A. Tarasenko, M. V. Entin, and L. I. Magarill, Valley separation in graphene by polarized light, *Phys. Rev. B* **84**, 195408 (2011).
- [19] F. Zhai and K. Chang, Valley filtering in graphene with a Dirac gap, *Phys. Rev. B* **85**, 155415 (2012).
- [20] Lü Xiao-Ling, Liu Zhe, Yao Hai-Bo, Jiang Li-Wei, Gao Wen-Zhu, and Zheng Yi-Song, Valley polarized electronic transmission through a line defect superlattice of graphene, *Phys. Rev. B* **86**, 045410 (2012).
- [21] D. Moldovan, M. Ramezani Masir, L. Covaci, and F. M. Peeters, Resonant valley filtering of massive Dirac electrons, *Phys. Rev. B* **86**, 115431 (2012).
- [22] Y. Jiang, T. Low, K. Chang, M. I. Katsnelson, and F. Guinea, Generation of Pure Bulk Valley Current in Graphene, *Phys. Rev. Lett.* **110**, 046601 (2013).
- [23] T. Cai, S. A. Yang, X. Li, F. Zhang, J. Shi, W. Yao, and Q. Niu, Magnetic control of the valley degree of freedom of massive Dirac fermions with application to transition metal dichalcogenides, *Phys. Rev. B* **88**, 115140 (2013).
- [24] M. M. Grujić, M. Ž. Tadić, and F. M. Peeters, Spin-Valley Filtering in Strained Graphene Structures with Artificially Induced Carrier Mass and Spin-Orbit Coupling, *Phys. Rev. Lett.* **113**, 046601 (2014).
- [25] L. Pratley and U. Zülicke, Valley filter from magnetotunneling between single and bi-layer graphene, *Appl. Phys. Lett.* **104**, 082401 (2014).
- [26] D. R. da Costa, Andrey Chaves, S. H. R. Sena, G. A. Farias, and F. M. Peeters, Valley filtering using electrostatic potentials in bilayer graphene, *Phys. Rev. B* **92**, 045417 (2015).
- [27] Zhe Liu, Liwei Jiang, and Yisong Zheng, Tunable valley polarization by a gate voltage when an electron tunnels through multiple line defects in graphene, *J. Phys.: Condens. Matter* **27**, 045501 (2015).
- [28] Changsoo Park, Generation of valley-polarized electron beam in bilayer graphene, *J. Appl. Phys.* **118**, 244301 (2015).
- [29] L. S. Cavalcante, A. Chaves, D. R. da Costa, G. A. Farias, and F. M. Peeters, All-strain based valley filter in graphene nanoribbons using snake states, *Phys. Rev. B* **94**, 075432 (2016).
- [30] S. P. Milovanović and F. M. Peeters, Strain controlled valley filtering in multi-terminal graphene structures, *Appl. Phys. Lett.* **109**, 203108 (2016).
- [31] M. Settnes, S. R. Power, M. Brandbyge, and A.-P. Jauho, Graphene Nanobubbles as Valley Filters and Beam Splitters, *Phys. Rev. Lett.* **117**, 276801 (2016).
- [32] F. Xu, Z. Yu, Y. Ren, B. Wang, Y. Wei, and Z. Qiao, Transmission spectra and valley processing of graphene and carbon nanotube superlattices with inter-valley coupling, *New J. Phys.* **18**, 113011 (2016).
- [33] D. R. da Costa, A. Chaves, G. A. Farias, and F. M. Peeters, Valley filtering in graphene due to substrate-induced mass potential, *J. Phys.: Condens. Matter* **29**, 215502 (2017).
- [34] Yee Sin Ang, Shengyuan A. Yang, C. Zhang, Zhongshui Ma, and L. K. Ang, Valleytronics in merging Dirac cones: All-electric-controlled valley filter, valve, and universal reversible logic gate, *Phys. Rev. B* **96**, 245410 (2017).
- [35] M. Settnes, J. H. Garcia, and S. Roche, Valley-polarized quantum transport generated by gauge fields in graphene, *2D Mater.* **4**, 031006 (2017).
- [36] T. Sekera, C. Bruder, E. J. Mele, and R. P. Tiwari, Switchable valley filter based on a graphene p - n junction in a magnetic field, *Phys. Rev. B* **95**, 205431 (2017).
- [37] Tayyaba Aftab, Valleytronics and phase transition in silicene, *Phys. Lett. A* **381**, 935 (2017).
- [38] Changsoo Park, Valley filtering due to orbital magnetic moment in bilayer graphene, *Phys. Lett. A* **382**, 121 (2018): [Related calculations of transmission probabilities in the presence of magnetic field can be found in this article.](#)
- [39] K. F. Mak, K. He, J. Shan, and T. F. Heinz, Control of valley polarization in monolayer MoS₂ by optical helicity, *Nat. Nanotechnol.* **7**, 494 (2012).
- [40] H. Zeng, J. Dai, W. Yao, D. Xiao, and X. Cui, Valley polarization in MoS₂ monolayers by optical pumping, *Nat. Nanotechnol.* **7**, 490 (2012).
- [41] Ting Cao, Gang Wang, Wenpeng Han, Huiqi Ye, Chuanrui Zhu, Junren Shi, Qian Niu, Pingheng Tan, Enge Wang, Baoli Liu, and Ji Feng, Valley-selective circular dichroism of monolayer molybdenum disulphide, *Nat. Commun.* **3**, 887 (2012).
- [42] Sanfeng Wu, Jason S. Ross, Gui-Bin Liu, Grant Aivazian, Aaron Jones, Zaiyao Fei, Wenguang Zhu, Di Xiao, Wang Yao, David Cobden, and Xiaodong Xu, Electrical tuning of valley magnetic moment through symmetry control in bilayer MoS₂, *Nat. Phys.* **9**, 149 (2013).
- [43] Anastasia Varlet, Ming-Hao Liu, Viktor Krueckl, Dominik Bischoff, Pauline Simonet, Kenji Watanabe, Takashi Taniguchi, Klaus Richter, Klaus Ensslin, and Thomas Ihn, Fabry-Pérot Interference in Gapped Bilayer Graphene with Broken Anti-Klein Tunneling, *Phys. Rev. Lett.* **113**, 116601 (2014): [The construction of potential profile, including barrier and well with band gap, using both top and bottom gates is explained in the Supplemental Material of this article.](#)
- [44] E. McCann and M. Koshino, The electronic properties of bilayer graphene, *Rep. Prog. Phys.* **76**, 056503 (2013).
- [45] Eduardo V. Castro, K. S. Novoselov, S. V. Morozov, N. M. R. Peres, J. M. B. Lopes dos Santos, Johan Nilsson, F. Guinea, A. K. Geim, and A. H. Castro Neto, Electronic properties of a biased graphene bilayer, *J. Phys.: Condens. Matter* **22**, 175503 (2010).
- [46] Yuanbo Zhang, Tsung-Ta Tang, Caglar Girit, Zhao Hao, Michael C. Martin, Alex Zettl, Michael F. Crommie, Y. Ron Shen, and Feng Wang, Direct observation of a widely tunable bandgap in bilayer graphene, *Nature* **459**, 820 (2009).
- [47] K. F. Mak, C. H. Lui, J. Shan, and T. F. Heinz, Observation of an Electric-Field-Induced Band Gap in Bilayer Graphene by Infrared Spectroscopy, *Phys. Rev. Lett.* **102**, 256405 (2009).
- [48] B. R. K. Nanda and S. Satpathy, Strain and electric field modulation of the electronic structure of bilayer graphene, *Phys. Rev. B* **80**, 165430 (2009).
- [49] J. N. Fuchs, F. Piéchon, M. O. Goerbig, and G. Montambaux, Topological Berry phase and semiclassical quantization of cyclotron orbits for two dimensional electrons in coupled band models, *Eur. Phys. J. B* **77**, 351 (2010).
- [50] Eduardo V. Castro, N. M. R. Peres, J. M. B. Lopes dos Santos, A. H. Castro Neto, and F. Guinea, Localized States at Zigzag Edges of Bilayer Graphene, *Phys. Rev. Lett.* **100**, 026802 (2008).

- [51] Eduardo V. Castro, N. M. R. Peres, J. M. B. Lopes dos Santos, F. Guinea, and A. H. Castro Neto, Bilayer graphene: Gap tunability and edge properties, *J. Phys.: Conf. Ser.* **129**, 012002 (2008).
- [52] Note that V_{g1} and V_{g2} are not the bare applied voltages. They are the band offset voltages determined by intrinsic carrier density due to doping and carrier density and asymmetry parameter, which are controlled by the applied top and back (or bottom) gate voltages: see Ref. [43] for details.
- [53] A. De Martino, L. Dell'Anna, and R. Egger, Magnetic barriers and confinement of Dirac-Weyl quasiparticles in graphene, *Solid State Commun.* **144**, 547 (2007).
- [54] Andrei V. Shytov, Mark S. Rudner, and Leonid S. Levitov, Klein Backscattering and Fabry-Pérot Interference in Graphene Heterojunctions, *Phys. Rev. Lett.* **101**, 156804 (2008).
- [55] M. I. Katsnelson, K. S. Novoselov, and A. K. Geim, Chiral tunnelling and the Klein paradox in graphene, *Nat. Phys.* **2**, 620 (2006).
- [56] Neetu Agrawal (Garg), Sankalpa Ghosh, and Manish Sharma, Electron optics with Dirac fermions: electron transport in monolayer and bilayer graphene through magnetic barrier and their superlattices, *Int. J. Mod. Phys. B* **27**, 1341003 (2013).
- [57] These choices are not necessary conditions for the valley-valve effect. When $E_\tau \neq E$ and $U \neq U_0 + U_m$ the transmission probability will be changed but the relative ratio η is still very large because of the suppressed transmission inside the band gap.
- [58] This may be compared to the magnetoresistance (MR) ratio of tunnel magnetoresistance or giant magnetoresistance.
- [59] As a numerical example, for $U_0 = 100$ meV, $d = 50$ nm (potential width), $B = 1$ T, and $W = 50$ nm (sample width) we have $k \simeq 0.2$ nm⁻¹, $\phi_c \simeq 54^\circ$, and $G_0 \simeq 4 \times 10^{-5}(1/\Omega)$.
- [60] C. S. Park, Band-gap tuned oscillatory conductance in bilayer graphene n - p - n junction, *J. Appl. Phys.* **116**, 033702 (2014).
- [61] Chang-Soo Park, Two-dimensional transmission through modified Poschl-Teller potential in bilayer graphene, *Phys. Rev. B* **92**, 165422 (2015).
- [62] H. Dery, P. Dalal, L. Cywiński, and L. J. Sham, Spin-based logic in semiconductors for reconfigurable large-scale circuits, *Nature* **447**, 573 (2007).
- [63] Wei Han, Roland K. Kawakami, Martin Gmitra, and Jaroslav Fabian, Graphene spintronics, *Nat. Nanotechnol.* **9**, 794 (2014).
- [64] Can Yesilyurt, Seng Ghee Tah, Gengchiao Liang, and Mansoor B. A. Jalil, Klein tunneling in Weyl semimetals under the influence of magnetic field, *Sci. Rep.* **6**, 38862 (2016).